Phys Chem Minerals (2003) 30: 230–242
DOI 10.1007/s00269-003-0304-8

ORIGINAL PAPER

R. Milke · R. Wirth

The formation of columnar fiber texture in wollastonite rims by induced stress and implications for diffusion-controlled corona growth

Received: 19 July 2002 / Accepted: 14 February 2003

Abstract The evolution of columnar fiber texture was studied in wollastonite reaction rims synthesized by the reaction calcite + quartz = wollastonite + CO_2. Experiments were performed at 850 to 950 °C at 100 MPa in dry CO_2 and were evaluated by scanning and transmission electron microscopy. Rim growth rates are interpreted as controlled by the diffusion of the SiO_2 component through the rims from the quartz–wollastonite to the wollastonite–calcite interface. The temperature dependence of rim growth rates yields an apparent activation energy of 314 ± 53 kJ mol^{-1}. The columnar fibrous wollastonite crystallizes at the quartz–wollastonite interface and comprises the largest parts of the rims. Ultimately, at the growth front strain contrast centers are present in the quartz. The strained volume extends about 200 nm into the quartz grains. We suggest that this might signify deformation of the quartz lattice due to wollastonite crystallization.

Wollastonite fiber thickness was measured from TEM images along traverses that represent intermediate positions of the growth front during the experiments. The average thickness is in the 100–200 nm range. Fiber thickness increases with increasing growth temperature. At a given temperature, the thickness of the fibers at the growth front slightly decreases with time, i.e., the number of fiber tips per unit area in the growth front increases. The decrease of the fiber thickness is well fitted by a parabolic rate law.

The generation of the columnar fiber texture is interpreted as an effect of induced stresses at the growth front, resulting from the volume increase due to the local reaction. This volume increase forces SiO_2 to diffuse along the growth front to the grain boundaries between the wollastonite fibers. These serve as fast diffusion pathways through the rims. The fiber thickness monitors the diffusion distances in the growth front and thus the height of the induced stress gradients. Since interface reactions are usually associated with volume changes, growth rates of reaction rims and zones in coronas are not only controlled by the diffusive mobility of the components but also by the volume restraints on the interface reactions.

R. Milke (✉) · R. Wirth
GeoForschungsZentrum Potsdam (GFZ),
Division 4, Telegrafenberg, 14473 Potsdam
Germany
e-mail: rmilke@gfz-potsdam.de

Introduction

Diffusion-controlled coronas are common textures in regional and contact metamorphic rocks, ranging from simple monomineralic rims to complex polymineralic coronas. They comprise well-defined mineral layers and sharp layer boundaries, arranged in a sequence of increasing or decreasing chemical potential (Fisher 1977). The rims or coronas separate phases that initially were in contact and were unstable under the P, T conditions of metamorphism. At the interfaces between different layers local equilibrium is usually assumed. The widths of the layers depend on the diffusive fluxes that can be estimated using nonequilibrium thermodynamics. The flux of each diffusing component is related to the chemical potential gradients and diffusion coefficients (e.g., Joesten 1977; Foster 1981; Ashworth and Birdi 1990; Johnson and Carlson 1990; Ashworth and Sheplev 1997). Reaction rims or coronas are useful indicators of diffusive transport, which in the μm to cm range is mostly achieved by grain boundary diffusion under the P, T conditions of metamorphism (Joesten 1991a). Thus, grain-boundary diffusion coefficients can be derived from measuring or estimating rim growth rates in experiments or using geological systems as natural laboratories (Joesten and Fisher 1988; Fisler and Mackwell 1994; Fisler et al. 1997; Yund 1997; Milke et al. 2001). They help understanding corona formation as well as a variety of metamorphic textures (Carlson 2002). Moreover, reaction rims and corona textures provide insight into the deviation from equilibrium conditions during metamor-

phism and its implications for geothermobarometry (Ashworth and Sheplev 1997; Ashworth et al. 1998).

Kinetic information is stored not only in mineral assemblages, layer sequences, and thickness, but also in the textures of reaction rims. There are a number of recurring patterns, for example symplectic layers, fibrous layers, or abrupt textural boundaries within mineral layers, all of which are important for the interpretation of rim growth. Symplectite layers consist of elongated intergrowths of different phases in equal spacing perpendicular to the reaction front at which they grew from a single reactant mineral. Examples of symplectite layers in reaction rims include symplectites of plagioclase–amphibole or plagioclase–amphibole–clinopyroxene (Carlson and Johnson 1991); amphibole–spinel (Mongkoltip and Ashworth 1983; Ashworth et al. 1992a); epidote–staurolite-spinel (Ashworth et al. 1992a); amphibole–garnet and clinopyroxene–garnet (Grant 1988); epidote–quartz (Ashworth et al. 1992b); orthopyroxene–garnet (Sack 1982); orthopyroxene–spinel (Joesten 1986; Ashworth and Sheplev 1997); scapolite–clinopyroxene (Abart et al. 2001), etc. Symplectite formation is explained by the presence of at least one immobile component that cannot diffuse farther in the reaction front than a half symplectite spacing as rim growth progresses. Thus, symplectic textures form by the action of chemical potential gradients in two directions: first, across the layers from interface to interface, and second, between the symplectite phases in the moving reaction front (Ashworth and Chambers 2000). Fibrous columnar textures consist of subparallel elongate crystals oriented perpendicular to the layer interfaces which occur in various types of monomineralic reaction rims or layers of coronas. They are frequent in wollastonite rims that grew around quartz inclusions in calcite or marble, and always occur in the parts of the rims adjacent to the quartz–wollastonite contact, either in contact aureoles (Joesten and Fisher 1988; Heinrich et al. 1995; Milke and Heinrich 2002) or in laboratory experiments (Milke and Heinrich 2002). The columnar wollastonite must not be confused with bundle-like aggregates of radiating fibers. Other examples of columnar fibrous layers in reaction rims include tilleyite layers as part of the sequence quartz | wollastonite| tilleyite| calcite in siliceous marbles (Joesten and Fisher 1988), diopside layers as part of the sequence orthopyroxene| diopside | garnet + diopside | plagioclase + sillimanite in metanorites (Attoh 1998), or orthopyroxene layers as part of the sequence olivine | orthopyroxene | orthopyroxene + garnet | plagioclase + K-feldspar in charnockites (Markl et al. 1998) and also as part of the sequence olivine | orthopyroxene | clinopyroxene | clinopyroxene + garnet | plagioclase in metagabbros (Grant 1988). There is evidence for a magmatic origin of columnar orthopyroxene layers in some coronas (de Haas et al. 2002); however, most columnar fibrous layers are clearly metamorphic. In both synthetic and natural wollastonite rims (Milke and Heinrich 2002) and in the tilleyite layers of Joesten and Fisher (1988) the columnar fibrous texture comprises only the inner part of the layers towards the core of the coronas. The outer part has granoblastic or radiating textures and is abruptly separated from the columnar fibrous zone. These textural discontinuities within mineral layers are interpreted as indicators of the position of the original interface between the reactants before rim growth (Joesten and Fisher 1988; Milke and Heinrich 2002). Obviously, these different textures within one layer are not determined by the inherent growth forms of the respective phases, but by the growth conditions at the interfaces. It is not clear why fiber textures evolve in many situations and what causes their formation. To better understand this process, we examined the fiber texture of synthetic wollastonite rims around quartz grains in calcite matrix, formed by the reaction

$$1\text{calcite} + 1\text{quartz} = 1\text{wollastonite} + 1CO_2. \quad (1)$$

Wollastonite formed in dry experiments, thus simulating pure thermal metamorphism of quartz-bearing marble. Reaction products were studied by scanning electron microscopy (SEM) and transmission electron microscopy (TEM). The TEM samples were prepared using the focused ion beam technique (FIB) (Overwijk et al. 1993). This new method allows the exactly localized preparation of TEM foils ($> 10 \times 10$ μm) from polished sections with constant thickness (e.g., 100 nm), even from inhomogeneous materials. The observations are discussed in the light of the various types of fiber textures known from rocks and rock-analogue synthetic products and the respective models for their formation. Our results suggest that the process leading to the growth of columnar fiber textures has basic implications for the theory of diffusion-controlled corona formation. We will point out the fundamental importance of volume changes and thereby induced stress fields on the scale of a single grain for the development of such textures. The results will help to better understand diffusion-controlled reaction fronts and to improve the prevailing models of reaction rim and corona growth.

Wollastonite rim growth in experiment and nature

The mechanism of the reaction quartz + calcite = wollastonite + CO_2 and the resulting morphology of wollastonite rims is different under dry and water-present conditions. If water is largely absent, wollastonite always overgrows and replaces quartz (Kridelbaugh 1973; Milsch 1999; Milke and Heinrich 2002). The rims are dense and have columnar fiber texture at the quartz–wollastonite interface. If pores are present on the SEM or TEM scale, they are restricted to the outer part of the rims near the wollastonite–calcite interface. If water is present in the fluid phase, wollastonite overgrows and replaces calcite (Kridelbaugh 1973; Tanner et al. 1985; Milke and Heinrich 2002). The rims have granoblastic texture, often are porous, and grow faster than the rims on quartz under the same P, T conditions. Natural wollastonite

rims from contact-metamorphic settings mirror these contrasting growth modes. Where stable isotope data indicate that rim growth occurred without infiltration of aqueous fluids, the wollastonite rims apparently replace quartz and form columnar fiber textures at the quartz–wollastonite interface (Olsen et al. 1992; Heinrich et al. 1995; Milke and Heinrich 2002). Kennedy (1959) gives an excellent example of pure thermal metamorphism of limestone nodules in quartzitic sandstone. Here, wollastonite replaces the quartz grains, preserving their shape. At the quartz–wollastonite contact the wollastonite has a columnar fiber texture perpendicular to the interface, whereas near the wollastonite–calcite contact sedimentary structures are obliterated and the wollastonite is coarse and granoblastic. Where, on the other hand, stable isotopes indicate that infiltration of aqueous magmatic fluids occurred, wollastonite replaces calcite at irregular reaction fronts and crystallizes with radial texture (Heinrich et al. 1995; Milke and Heinrich 2002). In both experiments and contact metamorphism the kinetics of the wollastonite-forming reaction is diffusion-controlled. Despite the large congruence between the textures of natural and synthetic wollastonite rims, the derived grain-boundary diffusion rates are 4 to 5 orders of magnitude larger during metamorphism than in the experiments (Milke and Heinrich 2002). The reasons for this discrepancy are unknown.

Experimental

Experiments were performed at 850, 900, and 950 °C at 100 MPa CO_2 pressure. The experiments used coarse quartz grains hot-pressed into a fine-grained calcite matrix. Pure, synthetic calcite (Merck) with grain sizes of 1–2 μm was used as calcite matrix. The quartz grains were split from clear Brazilian quartz crystals and sieved to 90–125 μm. The mixture consisted of about 15 vol% quartz and 85% calcite. It was dried at 120 °C and subsequently hot-pressed in a Paterson-type gas-medium apparatus at 300 MPa and 500 °C for 4 h. A porcelain-like reactant material resulted which was cut with a diamond saw into 1.5–2-mm-thick and 2–10-mm-long pieces. The pieces were placed in 3-mm-wide unsealed Pt capsules. Experiments were performed in conventional cold-seal pressure vessels with dry CO_2 (containing 0.009 wt% H_2O) as pressure medium. The hot-pressed samples thus were permanently in contact with the dry CO_2. By this method, the samples were effectively dried and the extremely low $X(H_2O)$ was very well controlled in all experiments. The method is identical to the experiments by Milke and Heinrich (2002), except that there most experiments were done with sealed capsules so that tiny amounts of adsorbed water had been trapped in the capsules. Temperature was measured with Ni–CrNi thermocouples situated inside the autoclaves directly adjacent to the central part of the Pt capsules. Total pressure and temperature uncertainties are estimated to be $< \pm 5$ °C and ± 10 MPa, respectively.

After the runs, the reaction products were embedded into epoxy and polished. The polished sections were examined by optical microscopy and SEM. For TEM, sections through the wollastonite rims were vertically cut from the polished surfaces using the focused ion beam method (FIB).

FIB preparation was performed in a FEI FIB 200 using a Ga^{3+} ion beam. The TEM foils with edge lengths of 10–12 μm were cut with a thickness of about 100 nm. They were lifted out using a glass capillary and placed on a copper grid. TEM investigations were carried out at 200 kV in a Philips CM200 electron microscope, equipped with a LaB_6 electron source. Series of TEM images made at 20 000× to 50 000× magnification in the bright-field mode and at various tilt angles in the dark-field mode were used to construct sketches of the rim textures. Measurements of fiber thickness were made from these sketches.

Results

SEM observations

The wollastonite rims always encase the quartz grains. The rims are separated from the calcite matrix by an open void that was filled with pressurized CO_2 during the experiments (Fig. 1). The voids around the reaction rims, together with isolated pores in the calcite matrix and tiny fluid inclusions in the outer parts of the rims, result from the CO_2 production and solid volume reduction of the reaction. The rims are texturally very similar to wollastonite rims that were produced in sealed capsules (Milke and Heinrich 2002). Figure 1a shows a quartz grain with a wollastonite rim from a sealed-capsule experiment (1000 °C; 100 MPa; 115 h). These rims are composed of two zones, a dense inner zone that has fibrous structure on the TEM scale and a porous, granoblastic outer zone. Milke and Heinrich (2002) explained the inner zone by replacement of quartz inwards from the original quartz–calcite interface and the outer zone by free growth outwards from the original interface into the surrounding void.

The wollastonite rims from the open capsule experiments are composed of a homogeneous zone of dense wollastonite entirely surrounding the quartz grains but are mostly lacking a continuous porous outer zone. On the flat faces of the quartz grains larger crystals or aggregates of crystals occur scattered on the dense wollastonite zone. At grain edges, however, the wollastonite rims are much thicker and CO_2-inclusion trails indicate that this thickening is due to localized crystallization of wollastonite that overgrows the dense rim (Fig. 1b; run conditions: 950 °C; 100 MPa; 48 h). The dense wollastonite zone has a very even thickness around the quartz grains. Only on a local scale at grain edges, did the overgrowing wollastonite apparently form a diffusion barrier and lead to slower growth of the inner zone (Fig. 1b, arrow 1). Between quartz and wollastonite there are no gaps or voids present except for cracks that formed subsequent to rim growth. Cracking of the quartz grains often cuts the wollastonite rims as well and probably occurred during quenching (Fig. 1a, arrow 1). Some of these cracks extend along the quartz–wollastonite interface (Fig. 1a, arrow 2). Where quartz grains were already cracked prior to rim growth, the cracks are partially filled by wollastonite and are marked by trails of CO_2 inclusions (Fig. 1b, arrow 2).

TEM observations

Figure 2a is a bright-field image of a complete TEM foil from run QC075 (950 °C; 100 MPa; 150 h) showing the

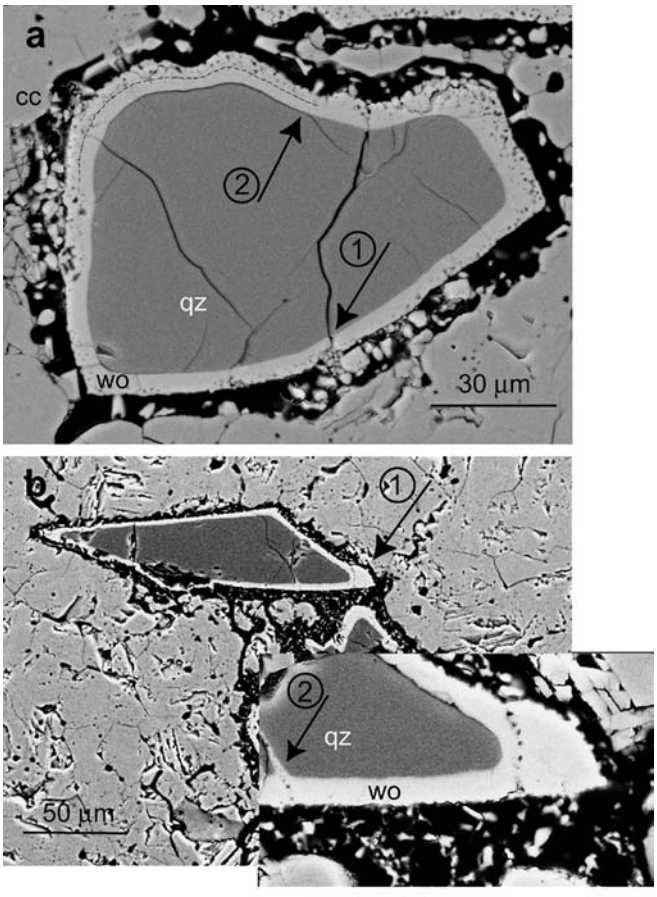

Fig. 1a, b BSE images of run products. The quartz grains are rimmed by wollastonite. The wollastonite rims are separated from the calcite matrix by a previously CO_2-filled void. **a** Wollastonite rim from a sealed-capsule-experiment (Milke and Heinrich 2002). The inner half of the rims is dense, while the outer half frequently bears small pores. The striated line in the *upper left corner* denotes the textural boundary. The commonly occurring cracks in the quartz grains have probably formed during quenching and often cut the wollastonite rims as well (*arrow 1*) or extend along the quartz–wollastonite interface (*arrow 2*). 100 MPa; 1000 °C; 115 h. **b** Wollastonite rim from an open-capsule experiment. The porous outer part of the rims is absent except for a patchy layer of granoblastic crystals. Bulky accumulations of granoblastic wollastonite have formed on grain edges (*arrow 1*). The rims are even in thickness except for localized thicker parts at exposed grain edges (*blowup*). Where cracking of the quartz grains occurred prior to rim growth, the cracks are filled with wollastonite and marked by a trail of pores (*arrow 2*). 100 MPa; 950 °C; 48 h

whole sequence quartz grain | wollastonite rim | void | calcite matrix. It corresponds to a position somewhere along the straight edges of the grain in Fig. 1b. This sample demonstrates the advantages of the FIB preparation method compared to conventional thinning of TEM foils. The three minerals have a very different resistance to the ion beam, so that it would not be possible to prepare such layer sequences with uniform thickness by conventional argon ion beam thinning. Constant thickness of the foil ensures uniform contrast conditions over the entire sample. Figure 2 shows that at TEM scale the quartz–wollastonite interface is smooth, and crystallographically determined interfaces are completely absent. Almost the entire wollastonite rim shows fiber texture with the elongated wollastonite grains oriented perpendicular to the quartz–wollastonite interface. The fibrous zone is overgrown by a patchy layer and local aggregates of rounded wollastonite crystals. All wollastonite crystals overgrowing the fiber zone have isometric habit. Since they have grown uninhibited into the CO_2-filled void, this must reflect the inherent growth form of wollastonite under the conditions of the experiments. In the central part of the micrograph a crack in the quartz grain is present that meets the quartz–wollastonite contact at an acute angle and then extends along the interface. Figure 2b (run QC071: 850 °C; 100 MPa; 150 h) is from a section of a wollastonite rim near a grain edge corresponding to the position of the blowup in Fig. 1b. Here, a clear separation exists between the fibrous zone at the quartz–wollastonite interface and the overgrown granoblastic zone. The elongated crystals at the quartz contact constitute approximately the innermost 500 nm of the rims. The thickness of individual crystals hardly exceeds 100 nm. In the granoblastic zone the crystals are considerably larger with diameters between 500 and 2000 nm.

Lattice symmetry and orientation of the crystals were determined by electron diffraction. The *d*-values indicate that the wollastonite occurs as the monoclinic 2M polytype. Various low index planes were identified in several orientations relative to the elongation of the fibers, suggesting that no preferred orientation exist. This finding replaces earlier assumptions (Milke and Heinrich 2002) that the elongation direction is parallel to the *b* axis, as is common in radial fibrous wollastonite aggregates.

Strain contrast centers (SCC) occur along the quartz–wollastonite interface, immediately located at the reaction front. The SCC appear in the bright-field image as a locally curved or bent diffraction contrast (indicated by arrows in Fig. 3a). They are known to be caused by local stress fields in the quartz lattice (Martin et al. 1996). Some of the lobes are centered around irregularities in the interface, like protruding crystal tips or embayments, but they also occur along the even parts of the interface (Fig. 3a). Diameters of individual SCC are about 200 nm. Diffraction contrast (dark lines in the bright-field image) in quartz parallel to the interface is undisturbed if its distance from the reaction front is 200 nm or more (Fig. 3b). No SCC were observed in the sample QC075. In this sample microcracks in quartz are present near or along the interface (Fig. 2a). If SCC have been present along the interface, it is possible that they relaxed during quenching due to microcrack formation.

Fiber thickness

The thickness of individual fibers was determined by the line-intercept method from the texture sketches after combining details from the series of bright-field and

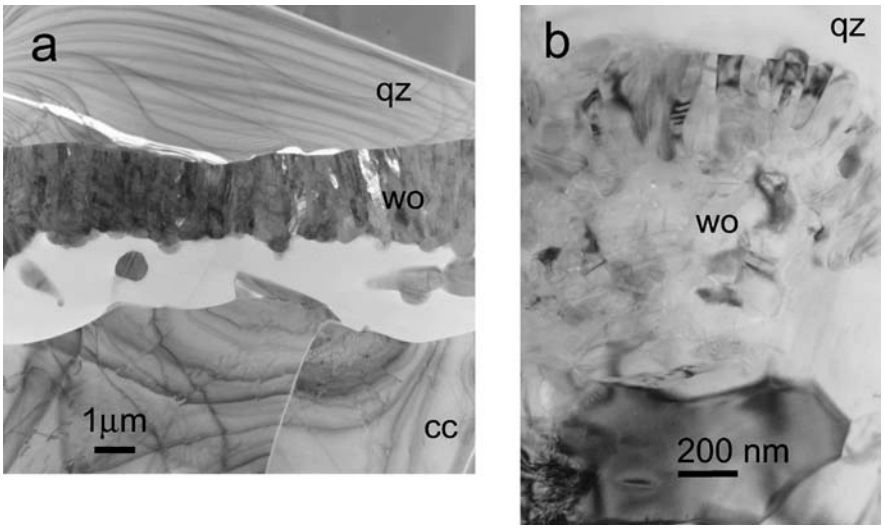

Fig. 2a, b TEM bright-field images of wollastonite rims from open-capsule experiments. **a** Complete section from the quartz grain through the wollastonite rim and open void into the calcite matrix. Foil thickness 100 nm. Run QC075; 100 MPa; 950 °C; 150 h. **b** Section from the quartz grain into the rim near a grain edge, where granoblastic wollastonite accumulated. Smooth quartz–wollastonite interface with sporadic protruding wollastonite fibers. At about 1/3 from the top, there is an abrupt contrast between the fiber texture and larger granoblastic wollastonite. Run QC071; 100 MPa; 850 °C; 150 h

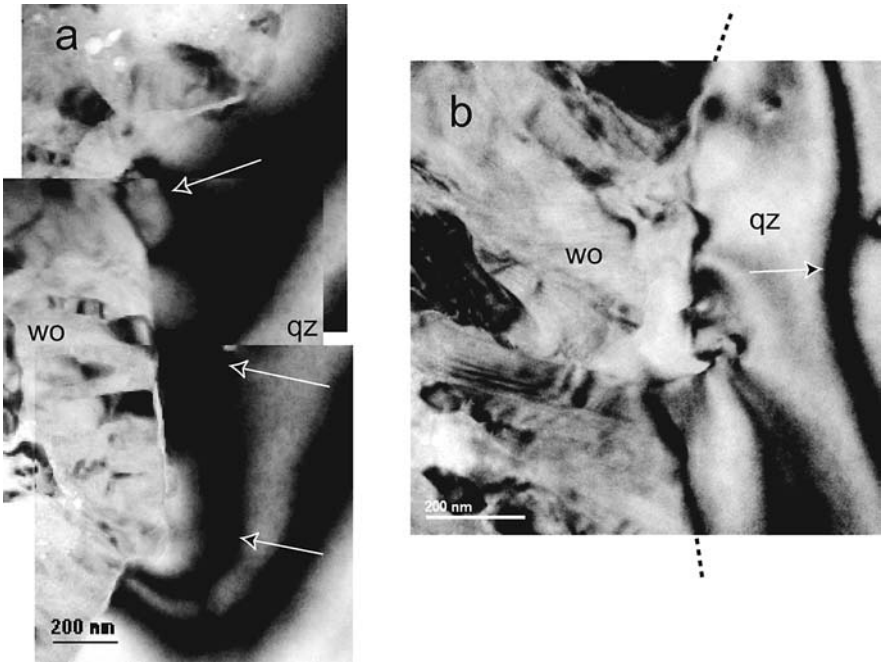

Fig. 3a, b TEM bright-field images of strain contrasts in quartz at the growth front. **a** Section of the quartz–wollastonite interface with a series of strain contrast centres (SCC), each about 200 nm in diameter. SCCs occur at protrusions, indentations, and flat parts of the growth front. Note that the strain contrast along the *right margin* of the picture is undisturbed. Run QC071; 100 MPa; 850 °C; 150 h. **b** Detail of the growth front with several small wollastonite protrusions that act as SCCs. The strain contrast along the *right margin* parallels the quartz–wollastonite interface at a distance of about 200 nm and is undisturbed from the SCCs. Run QC071; 100 MPa; 850 °C; 150 h

dark-field images (Fig. 4). Measurements were made along transects parallel to the quartz–wollastonite interface. These transect lines signify the former positions of the reaction front in intermediate stages of rim formation. For the reconstruction of rim growth we make use of the fact that during diffusion-controlled rim growth the rim thickness, X, increases parabolically with time (Fisher 1978):

$$X^2 = 2k \times t, \tag{2}$$

with k = parabolic rate constant and t = time. The validity of this rate law may safely be assumed, since both Milke and Heinrich (2002) and Milsch (1999) found parabolic increase of wollastonite rim thickness with time in isothermal experiments and no indication of an induction period for wollastonite rims on quartz grains. The oldest parts of the fibers, crystallized at $t = 0$, form the wall of the open voids or the textural boundary between the fibrous and granoblastic zones, respectively. We call them fiber roots. The youngest parts of the fibers, crystallized at $t = 150$ h, are the crystal tips in the reaction front, referred to as fiber tips. Results of transect measurements are given in Table 1. The evolution of fiber thickness from the original calcite–quartz ($t = 0$) to the quartz–wollastonite interface ($t = 150$ h) contains two remarkable observations (Fig. 5). First, the average fiber thickness, d_{av}, at the fiber tips increases with increasing growth temperature, from 88 nm (850 °C) to 165 nm (950 °C). Second, d_{av} decreases from the fiber roots to the fiber tips at each temperature. This decrease is larger at higher temperatures.

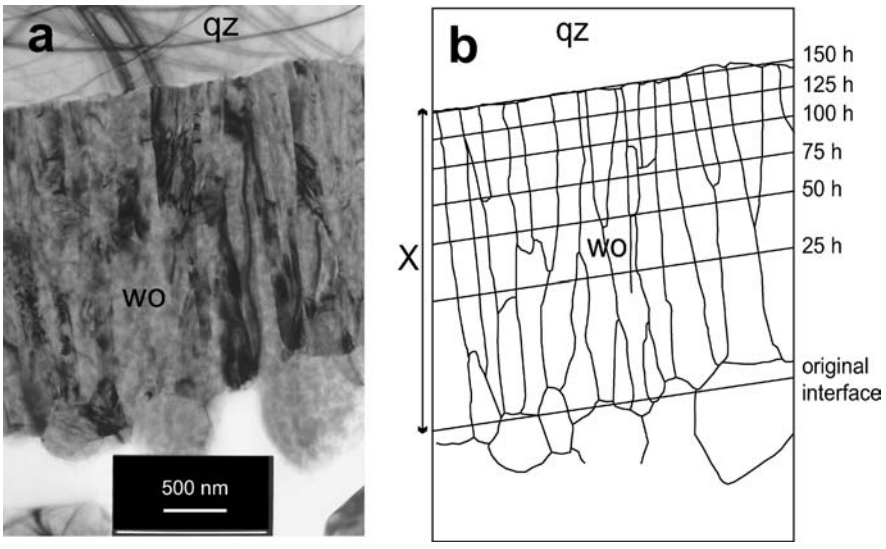

Fig. 4a, b Wollastonite rim and texture sketch. **a** Detail of the fibrous rim in Fig. 2a. The quartz–wollastonite interface is smooth with small undulations. At the opposite side, scattered granoblastic wollastonite crystals are overgrowing the fibrous zone. **b** Texture sketch as derived from a series of bright-field and dark-field images. Not all grain boundaries show up in **a**. The transect lines signify the position of the reaction front at intermediate stages

Table 1 Run conditions, rim thickness, grain-boundary diffusivity of SiO_2, initial and final average wollastonite fiber thickness (all experiments at $P = 100$ MPa in dry CO_2)

Run no.	T (°C)	t (h)	X (nm)[a]	$D'_{SiO_2}\delta$ ($m^3\ s^{-1}$)[b]	$d_{t=0}$ (nm)[c]	$d_{t=150}$ (nm)
QC071	850	150	560	5×10^{-27}	101	88
QC072	900	150	1020	2×10^{-26}	120	110
QC075	950	150	2180	1×10^{-25}	215	165

[a] X = rim width
[b] $D'_{SiO_2}\delta$ = grain-boundary diffusivity of SiO_2
[c] d = crystal thickness

Grain-boundary diffusion of the SiO_2 component

The TEM investigation of the reaction rims provides precise rim thickness measurements from which grain-boundary diffusion coefficients can be derived. Milke and Heinrich (2002) argued that the outward diffusion of the SiO_2 component from the quartz–wollastonite to the wollastonite–calcite interface is the rate-limiting step of the reaction. Assuming that starting from $t = 0$ the wollastonite rim thickness increased according to a parabolic rate law, grain-boundary diffusion coefficients for SiO_2 can be calculated from the rim thickness after 150 h using the method of Yund (1997). According to this method, the diffusivity of SiO_2 along the grain boundaries in the wollastonite rims is

$$D'_{SiO_2}\delta = dRTX^2\left[\pi\left(\sum v_{wo}/v_{SiO_2}\right)c_{SiO_2}V^M_{wo}\Delta\mu_{SiO_2}t\right]^{-1}, \quad (3)$$

with d = fiber thickness; (v_{wo}/v_{SiO_2}) = (stoich. coefficient of wollastonite in Eq. (1) / stoich. coefficient of SiO_2 in wollastonite) = 1; c_{SiO_2} = concentration of SiO_2 on grain boundaries, assumed to be identical to the concentration in wollastonite; V^M_{wo} = molar volume of wollastonite; $\Delta\mu_{SiO_2}$ = difference in chemical potential of SiO_2 between the qtz–wo and wo–cc interfaces. The $\Delta\mu_{SiO_2}$ values were calculated using the thermodynamic database of Gottschalk (1997). For d, the mean values of d_{av} at $t = 0$ and $t = 150$ h were used. Results are listed in Table 1 and shown in an Arrhenius plot in Fig. 6. The $D'_{SiO_2}\delta$ values are about a factor of 30–50 smaller than those derived from rims that have grown in sealed capsules and therefore in the presence of tiny traces of water that had been adsorbed to the sample surface before sealing. The values are also smaller by about 1 order of magnitude than those derived for rim growth in open capsules by Milke and Heinrich (2002) in experiments identical to those described here. This is due to the much higher precision of the rim thickness measurements from the TEM images and the smaller fiber thickness used in the calculations, coupled with the observation that only the fibrous part of the rim acted as a diffusion barrier. The new values yield an apparent activation energy of 314 ± 53 (2σ) kJ mol^{-1}, equal to the 330 ± 36 kJ mol^{-1} determined from wollastonite rim growth in sealed capsules (Milke and Heinrich 2002). This indicates that very tiny amounts of water (< 0.1 wt% in the samples) are enhancing the diffusion rates, but do not alter the diffusion mechanism of the rate-limiting species on the grain boundaries.

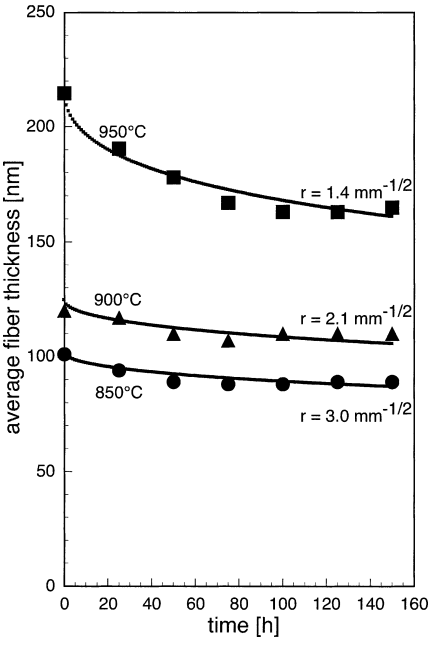

Fig. 5 Average fiber thickness vs. time for the three experiments at 850, 900, and 950 °C and least-squares fits according to Eq. (5). Values for r are the corresponding parabolic rate constants

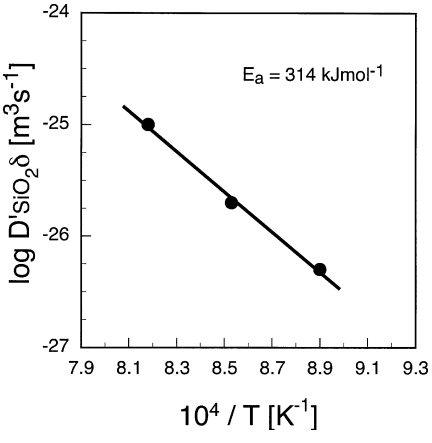

Fig. 6 Arrhenius plot of log SiO_2 diffusivity vs. $1/T$

Discussion

Fiber textures in rocks and synthetic rock analogues

The origin of fiber textures during diffusion-controlled rim and corona growth is discussed in the context of the various existing models for fiber growth developed for different geological environments. Some authors define fibrous textures as aggregates of extremely elongate parallel grains, with fiber shapes being unrelated to the crystallographic orientation and formed by minerals that normally do not grow in fibrous habit other than in these textures (Fisher and Brantley 1992). However, mostly, and also in this paper, "fiber texture" is used in a broader sense for all textures of (sub) parallel grains that are elongate in one dimension. This excludes radial fibrous aggregates.

There are models for columnar fiber growth into open space and in the absence of cavities. The most common mechanism for growth into open space is evolutionary selection during competitive crystallization. It occurs when crystals oriented with their fastest growth direction perpendicular to a substrate overgrow the less favorably oriented crystals. This mechanism was extensively used to explain fibrous textures in hydrothermal veins (Ramsay 1980; Cox and Etheridge 1983; Fisher and Brantley 1992), gypsum veins (Gustavson et al. 1994; El Tabakh et al. 1998), metallic and ceramic thin films (Van der Drift 1967; Muller 1985; Ying et al. 1996; Heydt et al. 2001), and other materials, and has been numerically modeled (Rodriguez-Navarro and Garcia-Ruiz 2000; Bons 2001; Hilgers et al. 2001).

Several models have been proposed for fiber growth in the absence of cavities. During localized dissolution-precipitation creep fibers grow during a continuous process by dissolution and nearby precipitation in a potential gradient (Durney and Ramsay 1973; Fisher and Brantley 1992; Bons and Jessell 1997). In rock environments this is mostly pressure solution and reprecipitation in the direction of the least compressive stress. As in the wollastonite rims, transport to and along the growth interface occurs by grain-boundary diffusion. The elongation of the fibers is independent of their crystallographic orientation. The fibers display a relatively constant width along their length. Fiber thickness in laboratory experiments under a temperature and concentration gradient in the grain boundary fluid was constant or slightly increasing in the growth direction (Bons and Jessell 1997). Similar mechanisms lead to fiber patterns in strain fringes that often occur associated with fibrous veins alongside rigid objects in deformed rocks (Ramsay and Huber 1983; Passchier and Trouw 1996; Koehn et al. 2000, 2001). A closely related mechanism is Taber growth, defined by Means and Li (2001) as the forceful growth of fibers at a macroscopically cohesive boundary between the fibers and a substrate through which the nutrients are delivered. Here, the fibers grow at their roots. Their growth entails no repeated cracking and sealing but the force of crystallization does work against the cohesion at the growth site.

A totally different approach was used to explain the self-organized crystallization of a siliceous medium to form agate by fiber growth at morphologically unstable crystallization fronts (Wang and Merino 1995; Merino et al. 1995). The gradient of fiber growth rate away from the crystallization front must be positive so that any small deviation from planarity tends to grow rather than dampen as time goes on. Initially present bumps on the front thus lengthen into fingers, each finger generating others nearby, and all of them become a coherent fiber texture.

The absence of preferred orientation in the wollastonite rims rules out that evolutionary selection is

responsible for their fiber texture. This is consistent with the diffusion-controlled growth kinetics, which implies that growth rates at any point in the reaction rims depend only on the diffusive fluxes of the nutrients and are independent of crystallographic directions. Crystallization at an unstable growth front also is not consistent with diffusion-controlled rim growth, since it requires a positive gradient of fiber growth rates away from the crystallization front. In diffusion-controlled layered aggregates, growth rates decrease parabolically with increased distance from the initial reaction front, thus leading to smooth instead of finger-like reaction fronts.

There is some analogy between fiber growth in the wollastonite rims and the Taber growth and dissolution-precipitation creep mechanisms. In the experiments the fibers formed in the absence of open space and the transport of nutrients to the growth sites occurred by diffusion through the solid medium. Similarly to the dissolution-precipitation creep experiments of Bons and Jessell (1997), where the fibers elongated along a concentration gradient in the grain boundary fluid, the elongation of the fibers is parallel to the chemical potential gradients $\Delta\mu_{CaO}$ and $\Delta\mu_{SiO_2}$. However, there are fundamental differences between the suggested fiber growth models and the growth of the fibrous wollastonite rims. The wollastonite grew by counter diffusion between the interfaces of the fibrous rims and not by dissolution of the material elsewhere and subsequent reprecipitation as fibers. The most significant difference is the evolution of the fiber thickness. While in all other models, as well as in natural or experimental observations, the fibers have equal or slightly increasing thickness in growth direction, in the wollastonite rims there is always a decrease. Two different scenarios can be used to explain this observation: (1) The number of fiber tips at the growth front and thus grain boundaries in the rim increased with time. The decrease in fiber thickness is a primary growth feature. (2) The fiber roots thickened due to grain growth, thus a secondary process subsequent to rim growth. In the following we will discuss what speaks for either of the two scenarios.

Did the fiber thickness increase by grain growth?

If the wollastonite coarsened due to grain growth, the older parts of the rims would have been annealed for a longer time than the younger parts, such that the wollastonite crystals should have ended up thickest at the original interface and thinnest at the growth front. Recrystallization and grain growth are known from metamorphic wollastonite rims. In the Christmas Mountains (Texas) contact aureole initially fibrous wollastonite recrystallized to a granoblastic polygonal texture, and in part of the aureole to porphyroblasts in a fine-grained matrix. Part of the fibrous wollastonite matrix remained in the interstices between the polygonal grains and coarsened with time. This matrix coarsening was interpreted as normal grain growth and oxygen diffusivity across the grain boundaries of 2×10^{-3} (ms^{-1}) exp ($-185/RT$) (kJ mol^{-1}) was derived (Joesten and Fisher 1988; Joesten 1991b). Granoblastic wollastonite in our synthetic rims formed only in the zone from the original interface to the wollastonite–calcite interface and no exaggerated grain growth was observed in the fibrous part of the rims. However, the fibers could still have been subject to normal grain growth.

Joesten (1985) argued that normal grain growth in silicates and oxides is controlled by oxygen diffusivity across the grain boundaries, $D'_{\text{øx}}/\delta$ ($D'_{\text{øx}}$ = oxygen grain boundary diffusion coefficient; δ = efficient grain boundary width). The question is if oxygen diffusion under the conditions of the experiments was fast enough to allow measurable coarsening of the wollastonite fibers and if the observed fiber thickness across the rim is consistent with grain growth.

Normal grain growth is described by the equation:

$$d^2 - d_0^2 = k \times t, \tag{4}$$

with d_0, d = initial and final grain diameters and k = constant proportional to D'_{ox}/δ (Joesten 1991b). Using k from Joesten and Fisher (1988; cf. Joesten 1991b) and d_0 from the fiber thickness at the growth front (Table 1), the fiber roots would have coarsened to a final thickness of 448 nm (850 °C), 645 nm (900 °C), and 936 nm (950 °C) after 150 h. All these values are much larger than measured, indicating that if normal grain growth was responsible for the variation in fiber thickness, oxygen diffusion must have been slower in the experiments than in the rocks. This is in accord with the variation in $D'_{SiO_2}\delta$ that is more than 6 orders of magnitude smaller in our dry experiments than in the rocks. Using $d^2 - d_0^2$ as measured, the k values would have to be 3.3×10^{-22} (850 °C), 2×10^{-22} (900 °C), and 4.7×10^{-21} (950 °C) m^2s^{-1} to account for the measured fiber thickness at the original interface, a factor of about 1000 smaller than determined from the coarsening of the metamorphic rims. Accordingly, $D'_{\text{øx}}/\delta$ would have to be 2 orders of magnitude smaller in the dry experiments than in the metamorphic rims. This could either be due to a decreased grain-boundary diffusion coefficient, $D'_{\text{øx}}$, or an increased effective grain-boundary width, δ, in the case of a wet grain-boundary.

How reasonable is this decrease in oxygen grain-boundary diffusivity, going from the contact metamorphism of cherts to a dry experiment? There are no experimental data on coarsening of wollastonite that could be used for an evaluation. However, as an analogy, coarsening and diffusion creep of quartz can be considered, where measured data is available for the cherts of the Christmas Mountains aureole as well as for "dry" and "wet" experiments. Coarsening of quartz in the Christmas Mountains aureole and experimental annealing of natural quartzite in the presence of 1–2 wt% H_2O (Tullis and Yund 1982; Pierce and Christie 1987) reveal essentially identical values for $D'_{\text{øx}}/\delta$ (Joesten 1991b). "Wet" experimental diffusion data therefore are a good

proxy for oxygen diffusion in the contact metamorphic rims. The effect of water can be assessed from steady-state creep measurements where arguably oxygen diffusion is rate-limiting as well (Joesten 1991a). Steady-state creep rates in vacuum dried quartzite are smaller by 3 orders of magnitude compared to "wet" quartzite (Jaoul et al. 1984). However, the deformation mechanism is dominated by Coble creep (controlled by grain-boundary diffusion) in the dry rock and by Nabarro–Herring creep (controlled by volume diffusion) in the water-bearing rock. The overall process is always controlled by the diffusion of the slower species on its faster path. Thus, if in fact oxygen diffusion were rate-limiting in both cases, this would imply that drying did decrease D'_{ox}/δ by less than 3 orders of magnitude. If the effect of water on oxygen diffusion across grain boundaries is similar in quartz and wollastonite, this would mean that D'_{ox}/δ in wollastonite during the dry rim growth experiments was less than 3 orders of magnitude smaller than in the contact metamorphic rims of the Christmas Mountains aureole. Thus, interpreting the increase in fiber thickness from tips to roots by normal grain growth would not conflict with realistic values for oxygen grain-boundary diffusivity. However, this reasoning involves a number of assumptions that may or may not be valid. There is no general agreement in the literature if, in fact, oxygen grain-boundary diffusion is generally rate-limiting in normal grain growth and in diffusion creep of silicates and oxides. It is uncertain if the rate-limiting diffusing component remains the same when the creep mechanism shifts from Coble creep in the dry rock to Nabarro–Herring creep in the presence of water. Moreover, it is not clear if the rate-determining species are the same for diffusion in quartz and wollastonite and if the effect of water is identical for both minerals. The discrepancy between the dry experiments and the metamorphic rims is several orders of magnitude larger for SiO_2 diffusion than the inferred effect on oxygen diffusion. Given the strong effect that even tiny amounts of water have on diffusion rates in the sealed compared to open capsule experiments, it might be problematic to infer the rim growth experiments from quartz deformation experiments.

The curvature of the fiber thickness vs. time curve (Fig. 5) suggests that the increase in fiber thickness at their roots may not be due to normal grain growth, since (according to Eq. 4) the rates of normal grain growth decrease with increasing grain diameter. The curves in Fig. 5 therefore would have to be steep on the right side (where the fibers are thin) and continually flatten towards the left side. In Fig. 7 it is shown how the fiber thickness would have evolved according to Eq. (4) with the fixed values of $d_{t=0}$ and $d_{t=150}$ taken from Table 1. The measured values diverge in a systematic way from the curves for the grain growth model. The observed shape of the thickness vs. time curves could only be achieved if the driving force for grain growth ceased during the course of rim growth. Two scenarios could potentially account for this: (1) the rate of grain growth for a given fiber thickness decreases with time and is practically zero during the second half of the experiments; (2) the rate of grain growth for a given initial thickness varies according to the position in the rim, with the largest growth rates at the outside of the rims and practically no grain growth in the innermost part of the rims where the fibers are thinnest. Both scenarios seem not physically probable in isobaric-isothermal experiments. We conclude that normal grain growth rates based on oxygen grain-boundary diffusion could theoretically account for the increase in fiber thickness, even though this requires several tacit assumptions already discussed. The shape of the fiber thickness vs. time curves, however, renders this interpretation improbable.

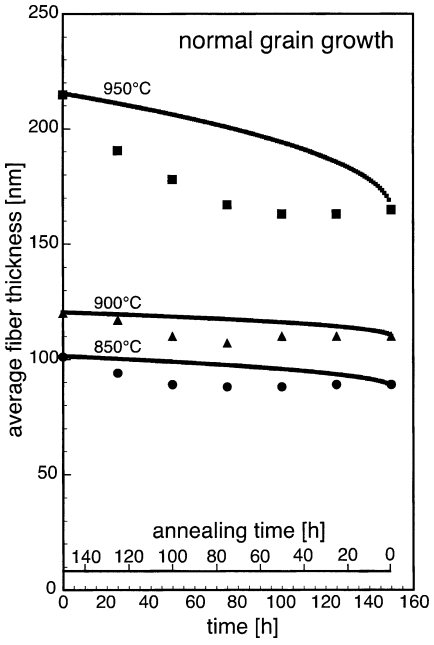

Fig. 7 Comparison between measured fiber thickness from Fig. (5) with model curves for normal grain growth calculated using Eq. (4) and taking the fixed values of $d_{t=0}$and $d_{t=150}$ from Table 1

While the fiber thickness might potentially be altered by grain growth, the thickness of the fiber tips is certainly not affected, since at the tips the annealing time is zero. Competitive nucleation and growth in confined space produces smaller crystals at higher overstepping. If the fiber thickness had evolved in a sequence of random nucleation, fiber growth, and grain growth, one would expect initially thinner fibers at increased temperatures due to a higher nucleation rate at the initial quartz–calcite interface, in contrast to the observations. The initial wollastonite crystal diameters should be preserved at the fiber tips throughout rim growth, as is typical for most of the discussed fiber textures. The increasing fiber thickness with higher temperatures indicates that it is controlled by a different mechanism. In the following we discuss the hypothesis that the thickness of the wollastonite fibers is controlled by induced stress at the growth front and the diffusivity of SiO_2 in the quartz–wollastonite interface.

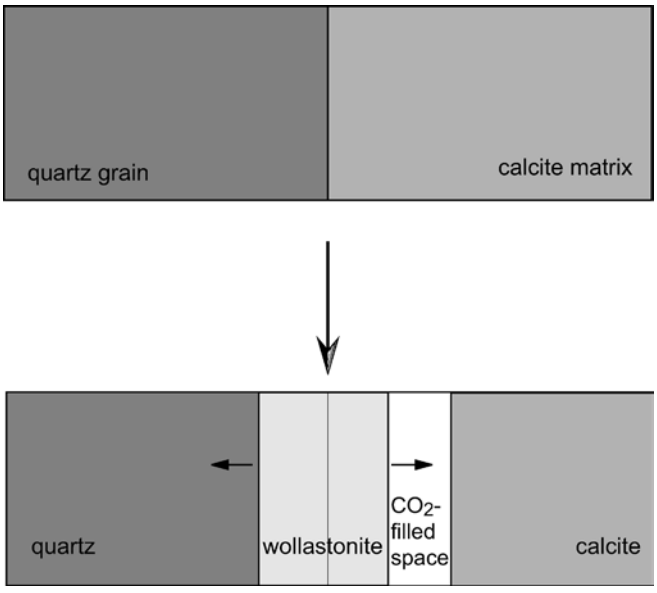

Fig. 8 Volume relations for wollastonite growth on quartz surfaces according to qz + cc = wo + CO_2. If volume-constant replacement of quartz by wollastonite occurs at the qz–wo interface, the position of the original interface is situated inside the rims and the wollastonite rim grows into two directions

Induced stress at the growth front

If wollastonite crystallizes at the quartz–wollastonite reaction front, a volume problem arises. The quartz consumed according to reaction (1) has only 0.57 times the volume of the produced wollastonite (Fig. 8). Wheeler (1987) pointed out that a volume increase at a reaction front inevitably induces local stresses. The initial stress normal to the reaction front will be smoothed out to a parabolic distribution of normal stresses around each grain that drive chemical fluxes along the interface, analogous to pressure solution-induced fluxes in monomineralic aggregates under normal stress (Rutter 1976). The dissolution or replacement of the reactant phase at the interface is thus coupled with the growth rate of the product phase. As a consequence, two phases cannot grow and dissolve at their mutual interface at independent rates but at rates determined by their specific volumes, stoichiometry, and phenomenological coefficients (Wheeler 1987). Carmichael (1986) followed a similar reasoning, pointing to the fact that any metasomatic reaction that would tend to change the volume is resisted by a local induced stress field. This induces secondary chemical potential gradients and drives secondary mass transfer. One way to release this induced stress could be deformation of the reaction rim and the surrounding matrix. It could also be released at a virtually constant pressure, provided diffusion allowed perfectly efficient secondary mass transfer through the reaction rim and the matrix. In this case, the reaction at the interface will be constrained very close to constant volume as material is transported in or out, which has long been identified as nature's common way of minimizing the induced stress fields during metasomatic reactions (Carmichael 1986). These ideas are corroborated by the wollastonite rim growth experiments. In the strain contrast in quartz along the wollastonite growth front (Fig. 3), reaction-induced stress fields become manifest. To our knowledge, this is the first example of reaction-induced stress fields made visible in a diffusion-controlled growth front. This interpretation implies that under the studied conditions the induced stress is not instantaneously released but builds up at the growth front. The strain contrast is reminiscent of strain contrast centers induced by electron irradiation damage in quartz, where local crystalline-to-noncrystalline transformation of quartz leads to local volume increase and distortions of the surrounding quartz lattice (Martin et al. 1996). The diameter of these strained lattice areas is around 200 nm, in the same range as observed along the growth front of the dry wollastonite rims.

Admittedly, other causes for the strain fields must be considered as well. In principal, they could have evolved either before rim growth during the hot pressing of the starting materials or after rim growth during the quenching of the runs. Their position at the actual growth front rules out that the strain resulted from the hot pressing. A more conceivable possibility is that the strain resulted from the different thermal contraction of quartz and wollastonite during quenching. This could be expected in a situation where one grain contracts less during cooling than the surrounding grains. However, the encased quartz grain decreases its volume by 4.3% from run temperature to room temperature (Carpenter et al. 1998), whereas the wollastonite rim, analogous to minerals of the pyroxene group, contracts by only about 2% (Demelza 1997; Pavese et al. 2000). Independent of the mutual orientation of the quartz and wollastonite grains, the volume decrease of quartz always exceeds that of wollastonite. Lattice distortion in the quartz grains due to cooling would require strong adhesion between the grains that leads rather to deformation of the quartz lattice than to the opening of minuscule gaps along the interfaces. The compaction of the matrix cannot have any effect on the reaction rims since the surrounding CO_2-filled pores cushion them.

If there were, in fact, a stress buildup at the growth front, its release would provide a driving force for the generation of new grain boundaries and thus new fibers. Interphase boundaries at a growth front are usually assumed to represent local equilibrium between the phases in mutual contact. Wheeler (1987) pointed out that reactions at a growth front always require diffusion along these interface boundaries, which in local equilibrium should be locked for diffusion, if not for the induced stress fields. From this model it follows that the diffusion distances along the reaction front are related to the thickness of the fiber tips and that therefore both should evolve as a function of the induced stress (Fig. 9). At each temperature there must be a characteristic initial diameter of the wollastonite crystals, now measured as d_{av} at the fiber roots. If this idea is correct, the number

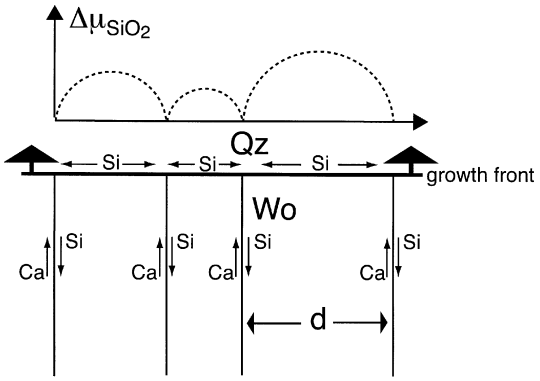

Fig. 9 Induced chemical potential gradients and diffusion paths at the reaction front. The *thick arrows* indicate the propagation direction. CaO must diffuse into the reaction front, and the slower SiO_2 out. The thicker the fiber tips, the higher is the required potential difference, $\Delta\mu_{SiO_2}$, to allow steady-state diffusion along the qz–wo interface and through the wo rims

of fibers in a unit area should increase during rim growth together with the decreasing force of crystallization as a parabolic function of time. To test this idea, the thickness vs. time values (Fig. 5) were fitted to the equation:

$$A = nd^2 + rt^{1/2}d^2, \quad (5)$$

with A = unit area in the growth front; n = initial number of fiber tips in the unit area; d = fiber thickness; r = parabolic rate constant for the generation of new fibers. Using a least-squares fit for r according to Eq. (5), the number of fiber tips in a unit area of the growth front increases in the range between 38% (850 °C) and 59% (950 °C) in 150 h. The total length of wollastonite–wollastonite grain boundaries at the growth front increases with the square root of the number of fiber tips, thus in the range between 17% (850 °C) and 26% (950 °C). The absolute increase in wollastonite–wollastonite grain-boundary length in the growth front is larger at 850 °C than at 950 °C, due to its larger initial size. Normalized to the increase at 950 °C, the increase in grain boundary length in the growth front at 850, 900, and 950 °C assumes values of 1.6, 1.3, and 1. Thus, despite the slower rim growth, the increase in the wo–wo grain-boundary area is larger at lower than at higher temperatures. Relating the increase in grain-boundary length in the growth front to the rim growth rates, the generation of grain-boundary area is 6.2 times faster at 850 than at 950 °C and 2.4 times faster at 900 than at 950 °C. This result is well in accordance with our model. One may assume that the diffusivity of SiO_2 in the quartz–wollastonite interfaces lies in a range similar to that in wollastonite grain boundaries and that the activation energy for diffusion in both situations is similar (Farver and Yund 1995). From 950 to 850 °C, the SiO_2 diffusivity decreases by a factor of 20. However, the rim growth rate and thus the propagation of the growth front decreases by a factor of only 4 (Table 1). It must therefore be increasingly difficult at lower temperature for the stressed reaction front to release this stress by diffusion along and out of the interface. Consequently, more energy should be stored at the reaction front in the form of strain energy in quartz and interface energy in wollastonite.

As rim growth progresses, the growth rates parabolically decrease with time, and accordingly also the steady-state diffusion rates along the growth front as well as the stress-inducing force of crystallization. If the grains were totally inelastic, the decreasing diffusion rates and declining induced stress gradients should exactly level off, so that continuous growth could evolve with constant fiber thickness. As the measurements show, this is not the case. Obviously the induced stress gradients cannot keep up with the rates of diffusion across the rims, such that the generation of new grain boundaries is necessary to compensate for the shortened diffusion distances in the reaction front. Possibly this is due to the loss of induced stress as elastic strain energy into the quartz grains, as evident in the form of the SCCs.

According to this model, the generation of columnar fiber textures in diffusion-controlled rim growth is similar to models for symplectite formation in reaction rims (Ashworth and Chambers 2000). In both situations, the thickness of the elongated product grains is explained by restricted diffusion along chemical potential gradients in the reaction front. While potential gradients between symplectite phases result from their different chemical compositions, they result from induced stresses in the monomineralic fiber textures. However, if our model for the generation of fiber textures in reaction rims is correct, there is no reason why induced stresses should not play a role in the development of symplectic textures as well.

Consequences

According to our interpretation, the columnar fiber texture in the wollastonite rims results from a growth front working against a volume restraint. Such conditions should occur at other diffusion-controlled reaction fronts as well, either in monomineralic reaction rims or layers of zoned coronas. It is likely that columnar fibrous layers in diffusion-controlled reaction textures generally indicate release of crystallization-induced stresses. Carmichael (1986) pointed out the consequences that induced stress and secondary mass transport have for the theory of diffusion metasomatism. Due to secondary transport, the evolution of diffusion-controlled coronas is not defined by the primary chemical potential gradients and the diffusivities of the various components alone, but to the same degree by the volume restraint. The original quantitative theory of metasomatic rim growth (Joesten 1977) has undergone various extensions, the most important of which is the allowance for component fluxes beyond the boundaries of the reaction rims (Johnson and Carlson 1990). However, even in recent studies the formation of diffusion-controlled corona textures is still modeled without explicitly considering the effects of volume

changes. Our results strongly support the idea of induced stresses and secondary mass transfer. If this is correct, it is essential to include into corona growth models the effects from volume changes and nature's tendency towards volume preservation.

An important consequence of the volume argument is the coupling of the diffusion fluxes of several components, independent of what their diffusivities were, without a volume restraint. Since the volume changes are different at each reaction front in a corona, the phenomenological coefficients for diffusion of the components will not be constant, but differ from layer to layer.

In the simple case of a monomineralic wollastonite rim encasing a quartz grain there is no volume restriction for the outward diffusion of SiO_2 away from the growth front through the rim. The inward diffusion of CaO from the calcite–wollastonite interface to the growth front, however, is restricted to the volume made available by consumption of quartz at the wollastonite–quartz interface. For this reason the CaO diffusion is controlled by the SiO_2 diffusion (Milke and Heinrich 2002). In contrast, volume changes were not considered in the interpretation of wollastonite rims in the Christmas Mountains aureole and therefore the diffusion fluxes of the SiO_2 and CaO components were treated as being independent (Joesten and Fisher 1988). This led to the result that the volume of the produced wollastonite was larger than the volume of the consumed quartz at the quartz–wollastonite interface. This would not be possible in a system under constant pressure. Stresses would have built up at the reaction front, deforming the wollastonite rims and the surrounding marble matrix. These processes would have strongly affected the effective pressures at the interfaces and the energy budget of the reaction. It is emphasized that the wollastonite formation has to work against a volume restraint although the overall reaction has a negative ΔV with respect to the solids and produces porosity remote from the reaction front.

Future experimental work is needed to assess the importance of strain and deformation energy during corona growth in terms of the total energy budget. Realistic models must include volume restraints and allow induced stresses to be released by secondary transport. Columnar fibrous layers indicate crystallization against a volume restraint and therefore define boundary conditions for the respective reactions at the interfaces.

Acknowledgements We thank two anonymous reviewers for their criticism and support, W. Heinrich and M. Gottschalk for discussions during the progress of the study, E.M. Schemmert for preparatory work, and D. Harlov for language improvements. A. Schertel did FIB preparation at the FEI Laboratories in Feldkirchen, Germany.

References

Abart R, Schmud R, Harlov D (2001) Metasomatic coronas around hornblendite xenoliths in granulite facies marble, Ivrea zone, N Italy, I: constraints on component mobility. Contrib Mineral Petrol 141: 473–493

Ashworth JR, Birdi JJ (1990) Diffusion modelling of coronas around olivine in an open system. Geochim Cosmochim Acta 54: 2389–2401

Ashworth JR, Chambers AD (2000) Symplectic reaction in olivine and the controls of intergrowth spacing in symplectites. J Petrol 41: 285–304

Ashworth JR, Sheplev VS (1997) Diffusion modelling of metamorphic layered coronas with stability criterion and consideration of affinity. Geochim Cosmochim Acta 61: 3671–3689

Ashworth JR, Sheplev VS, Bryxina NA, Kolobov VY, Reverdatto VV (1998) Diffusion-controlled corona reaction and overstepping of equilibrium in a garnet granulite, Yenisey Ridge, Siberia. J Metam Geol 16: 231–246

Ashworth JR, Birdi JJ, Emmett TF (1992a) A complex corona between olivine and plagioclase from the Jotun Nappe, Norway, and the diffusion modelling of multimineralic layers. Min Mag 56: 511–525

Ashworth JR, Birdi JJ, Emmett TF (1992b) Diffusion in coronas around clinopyroxene: modelling with local equilibrium and steady state, and a non-steady-state modification to account for zoned actinolite-hornblende. Contrib Mineral Petrol 109: 307–325

Attoh K (1998) Models for orthopyroxene-plagioclase and other corona reactions in metanorites, Dahomeyide orogen, West Africa. J Metam Geol 16: 345–362

Bons PD (2001) Development of crystal morphology during unitaxial growth in a progressively widening vein: I. The numerical model. J Struct Geol 23: 865–872

Bons PD, Jessell MW (1997) Experimental simulation of the formation of fibrous veins by localised dissolution-precipitation creep. Miner Mag 61: 53–63

Carlson WD (2002) Scales of disequilibrium and rates of equilibration during metamorphism. Am Mineral 87: 185–204

Carlson WD, Johnson CD (1991) Coronal reaction textures in garnet amphibolites of the Llano Uplift. Am Mineral 76: 756–772

Carmichael DM (1986) Induced stress and secondary mass transfer: thermodynamic basis for the tendency toward constant-volume constraint in diffusion metasomatism. In: Helgeson HC (ed) Chemical transport in metasomatic processes. NATO ASI series C 218, Reidel, Dordrecht, pp 239–264

Carpenter MA, Salje EKH, Graeme-Barber A, Wruck B, Dove MT, Knight KS (1998) Calibration of excess thermodynamic properties and elastic constant variations associated with the $\alpha \leftrightarrow \beta$ phase transition in quartz. Am Mineral 83: 2–22

Cox SF, Etheridge MA (1983) Crack-seal fibre growth mechanisms and their significance in the development of oriented layer silicate microstructures. Tectonophysics 92: 147–170

de Haas GJL, Nijland TG, Valbracht PJ, Maijer C, Verschure R, Andersen T (2002) Magmatic versus metamorphic origin of olivine-plagioclase coronas. Contrib Mineral Petrol 143: 537–550

Demelza HJ (1997) Thermal expansion of $MgSiO_3$ and $FeSiO_3$ ortho- and clinopyroxenes. Am Mineral 82: 689–696

Durney DW, Ramsay JG (1973) Incremental strains measured by syntectonic crystal growths. In: De Jong KA, Scholten R (eds) Gravity and tectonics. Wiley, New York pp 67–96

El Tabakh M, Schreiber BC, Warren JK (1998) Origin of fibrous gypsum in the Newark Rift Basin, eastern North America. J Sedim Res 68: 88–99

Farver JR, Yund RA (1995) Interphase boundary diffusion of oxygen and potassium in K-feldspar/quartz aggregates. Geochim Cosmochim Acta 59: 3697–3705

Fisher DM, Brantley SL (1992) Models of quartz overgrowth and vein formation: deformation and episodic fluid flow in an ancient subduction zone. J Geophys Res 97: 20043–20061

Fisher GW (1977) Nonequilibrium thermodynamics in metamorphism. In: Fraser DG (ed) Thermodynamics in geology. Reidel, Dordrecht, pp 381–403

Fisher GW (1978) Rate laws in metamorphism. Geochim Cosmochim Acta 42: 1035–1050

Fisler DK, Mackwell SJ (1994) Kinetics of diffusion-controlled growth of fayalite. Phys Chem Mineral 21: 156–165
Fisler DK, Mackwell SJ, Petsch S (1997) Grain boundary diffusion in enstatite. Phys Chem Mineral 24: 264–273
Foster CT Jr. (1981) A thermodynamic model of mineral segregations in the lower sillimanite zone near Rangeley, Maine. Am Mineral 66: 260–277
Gottschalk M (1997) Internally consistent thermodynamic data for rock forming minerals in the system SiO_2–TiO_2–Al_2O_3–Fe_2O_3–CaO–MgO–FeO–K_2O–Na_2O–H_2O–CO_2. Europ J Mineral 9: 175–223
Grant SM (1988) Diffusion models for corona formation in metagabbros from the Western Grenville Province, Canada. Contrib Mineral Petrol 98: 49–63
Gustavson TC, Hovorka SD, Dutton AR (1994) Origin of satin spar veins in evaporite basins. J Sediment Res A64: 88–94
Heinrich W, Hoffbauer R, Hubberten HW (1995) Contrasting fluid flow patterns at the Bufa del Diente contact metamorphic aureole, north-east Mexico: evidence from stable isotopes. Contrib Mineral Petrol 119: 362–376
Heydt P, Luo C, Clarke DR (2001) Crystallographic texture and thermal conductivity of zirconia thermal barrier coatings deposited on different substrates. J Am Ceram Soc 84: 1539–1544
Hilgers C, Koehn D, Bons PD, Urai JL (2001) Development of crystal morphology during unitaxial growth in a progressively widening vein II: Numerical simulations of the evolution of antitaxial fibrous veins. J Struct Geol 23: 873–885
Jaoul O, Tullis, Kronenberg A (1984) The effect of varying water contents in the creep behavior of Heavitree quartzite. J Geophys Res 89: 4298–4312
Joesten R (1977) Evolution of mineral assemblage zoning in diffusion metasomatism. Geochim Cosmochim Acta 41: 649–670
Joesten R (1985) A diffusion-compensation relation for normal grain growth and grain-boundary diffusion of oxygen in oxides. J Am Ceram Soc 68, C62–C64
Joesten R (1986) The role of magmatic reaction, diffusion and annealing in the evolution of coronitic microstructure in troctolitic gabbro from Risör, Norway. Min Mag 50: 441–467
Joesten R (1991a) Grain-boundary diffusion kinetics in silicate and oxide minerals. In: Ganguly J (ed) Diffusion, atomic ordering, and mass transport. Springer, Berlin Heidelberg New York, pp 345–395
Joesten (1991b) Kinetics of coarsening and diffusion-controlled mineral growth. In: Kerrick DM (ed) Contact metamorphism. Reviews in Mineralogy, vol 26, Washington, DC, pp 507–582
Joesten R, Fisher G (1988) Kinetics of diffusion-controlled mineral growth in the Christmas Mountains (Texas) contact aureole. Geol Soc America Bull 100: 714–732
Johnson CD, Carlson WD (1990) The origin of olivine-plagioclase coronas in metagabbros from the Adirondack Mountains, New York. J Metam Geol 8: 697–717
Kennedy (1959) The formation of a diffusion reaction skarn by pure thermal metamorphism. Min Mag 32: 26–31
Koehn D, Hilgers C, Bons PD, Passchier CW (2000) Numerical simulation of fibre growth in antitaxial strain fringes. J Struct Geol 22: 1311–1324
Koehn D, Aerden DGAM, Bons PD, Passchier CW (2001) Computer experiments to investigate complex fibre patterns in natural antitaxial strain fringes. J Metam Geol 19: 217–231
Kridelbaugh SJ (1973) The kinetics of the reaction: calcite + quartz = wollastonite + carbon dioxide at elevated temperatures and pressures. Am J Sci 273: 757–777
Markl G, Foster CT, Bucher K (1998) Diffusion-controlled olivine corona textures in granitic rocks from Lofoten, Norway: calculation of Onsager diffusion coefficients, thermodynamic modelling and petrological implications. J Metam Geol 16: 607–623
Martin B, Flörke OW, Kainka E, Wirth R (1996) Electron irradiation damage in quartz, SiO_2. Phys Chem Miner 23: 409–417
Means WD, Li T (2001) A laboratory simulation of fibrous veins: some first observations. J Struct Geol 23: 857–863
Merino E, Wang Y, Deloule E (1995) Genesis of agates in flood basalts: twisting of chalcedony fibers and trace-element geochemistry. Am J Sci 295: 1156–1176
Milke R, Heinrich W (2002) Diffusion-controlled growth of wollastonite rims between quartz and calcite: comparison between nature and experiment. J Metam Geol 20: 467–480
Milsch H (1999) Experimentelle Untersuchung des Einflusses von Dekarbonatisierungsreaktionen auf die Transporteigenschaften von Gesteinen. PhD dissertation, University Potsdam, Germany, 126 p
Mongkoltip P, Ashworth JR (1983) Quantitative estimation of an open-system symplectite-forming reaction: restricted diffusion of Al and Si in coronas around olivine. J Petrol 24: 635–661
Muller K-H (1985) Dependence of thin-film microstructure on deposition rate by means of a computer simulation. J Appl Phys 58: 2573–2576
Olsen SN, Baumgartner LP, Brown PE (1992) Possible prograde fluid inclusions in recrystallized chert nodules in a contact aureole, Christmas Mountains, Texas. Am Mineral 77, 1031–1037
Overwijk MHF, van den Heuvel FC, Bulle-Lieuwma CWT (1993) Novel scheme for the preparation of transmission electron microscopy specimens with the focused ion beam. J Vac Sci Technol 11, 202
Passchier CW, Trouw RAJ (1996) Microtectonics. Springer Berlin Heidelberg New York, 289 p
Pavese A, Bocchio R, Ivaldi G (2000) In situ high temperature single crystal X-ray diffraction study of a natural omphacite. Mineral Mag 64: 983–993
Pierce ML, Christie JM (1987) Kinetics of grain growth in quartz aggregates. EOS Trans 68: 422
Ramsay JG (1980) The crack-seal mechanism of rock deformation. Nature 284: 135–139
Ramsay JG, Huber MI (1983) The techniques of modern structural geology, 1: Strain analysis. Academic Press, London
Rodriguez-Navarro A, Garcia-Ruiz JM (2000) Model of textural development of layered crystal aggregates. Eur J Mineral 12: 609–614
Rutter EH (1976) The kinetics of rock deformation by pressure solution. Phil Trans Roy Soc (A) 283: 203–219
Sack RO (1982) Reaction skarns between quartz-bearing and olivine-bearing rocks. Am J Sci 282: 970–1011
Tanner SB, Kerrick DM, Lasaga AC (1985) Experimental kinetic study of the reaction: calcite + quartz = wollastonollastonite + carbon dioxide, from 1 to 3 kbars and 500 to 850 °C. Am J Sci 285: 577–620
Tullis J, Yund RA (1982) Grain growth kinetics of quartz and calcite aggregates. J Geol 90: 301–318
Van der Drift A (1967) Evolutionary selection, a principle governing growth orientation in vapour-deposited layers. Philips Res Rep 22: 267–288
Wang Y, Merino E (1995) Origin of fibrosity and banding in agates from flood basalts. Am J Sci 295: 49–77
Wheeler J (1987) The significance of grain-scale stresses in the kinetics of metamorphism. Contrib Mineral Petrol 97: 397–404
Ying F, Smith RW, Srolovitz DJ (1996) The mechanism of texture formation during film growth: the roles of preferential sputtering and shadowing. Appl Phys Lett 69: 3007–3009
Yund RA (1997) Rates of grain boundary diffusion through enstatite and forsterite reaction rims. Contrib Mineral Petrol 126: 224–236